Cloud Phase Determination in the Arctic Using AERI Data

D. D. Turner and S. A. Ackerman
Cooperative Institute for Meteorological Satellite Studies
University of Wisconsin - Madison
Madison, Wisconsin

Introduction

Cloud-radiative processes in the Arctic have a large and significant effect on the global energy budget. Curry et al. (1996) have identified cloud phase as one of the primary unknowns, which affects the radiation budget in the Arctic. To correctly determine cloud properties, such as particle size and condensed water path that dictate the cloud's radiative effects, the cloud phase must be accurately determined. However, the presence of highly reflecting snow and ice, together with a persistent temperature inversion that exists much of the year, hampers the ability to remotely detect cloud phase. This paper demonstrates that far-infrared observations (between 17 to 20 μm) can help resolve ambiguities and improve infrared (IR) cloud phase detection.

Approach

In the IR, the refractive indices of liquid water and ice vary dramatically with wavelength, as shown in Figure 1. Many studies (e.g., Baum et al. 2000) have taken advantage of the differences in the imaginary refractive indices of water and ice between 8 and 12 μm to ascertain cloud phase. However, as shown in Figure 1, the indices of refraction are significantly different at 17-20 μm, with liquid water being more absorptive than ice. Using data from this wavelength region, together with observations at 8 and 12 μm, offers more information for accurate phase determination. The ground-based Atmospheric Emitted Radiance Interferometers (AERIs), deployed during Surface Heat Budget of the Arctic Ocean (SHEBA), and currently at the Atmospheric Radiation Measurement (ARM) North Slope of Alaska (NSA) site, have been extended such that high-quality measurements can be made at these long wavelengths (i.e., at 18-24 μm).

We have investigated the ability to ascertain cloud phase by using downwelling brightness temperature observations at 9, 12, and 18 μm. Using gaseous optical depths calculated from the Line-by-Line Radiative Transfer Model (LBLRTM), a range of mixed phase clouds were simulated using discrete ordinate radiative transfer (DISORT). The total optical depth of the clouds ranged from 0.1 to 8, and the fraction of liquid water in the cloud ranged from 0 (all ice) to 1 (all liquid water) by increments of 0.1. This data was used to build an algorithm to identify the cloud phase. The simulation and the results of the cloud phase detection algorithm are shown in Figure 2. For this simulation, the cloud particles were uniformly mixed, although using adjacent layers (i.e., an ice cloud directly above a liquid water cloud or vice versa) does not significantly affect the results. The effective radius used for the liquid water droplets and ice crystals in this simulation is 7 μm and 21 μm, respectively, according to in situ

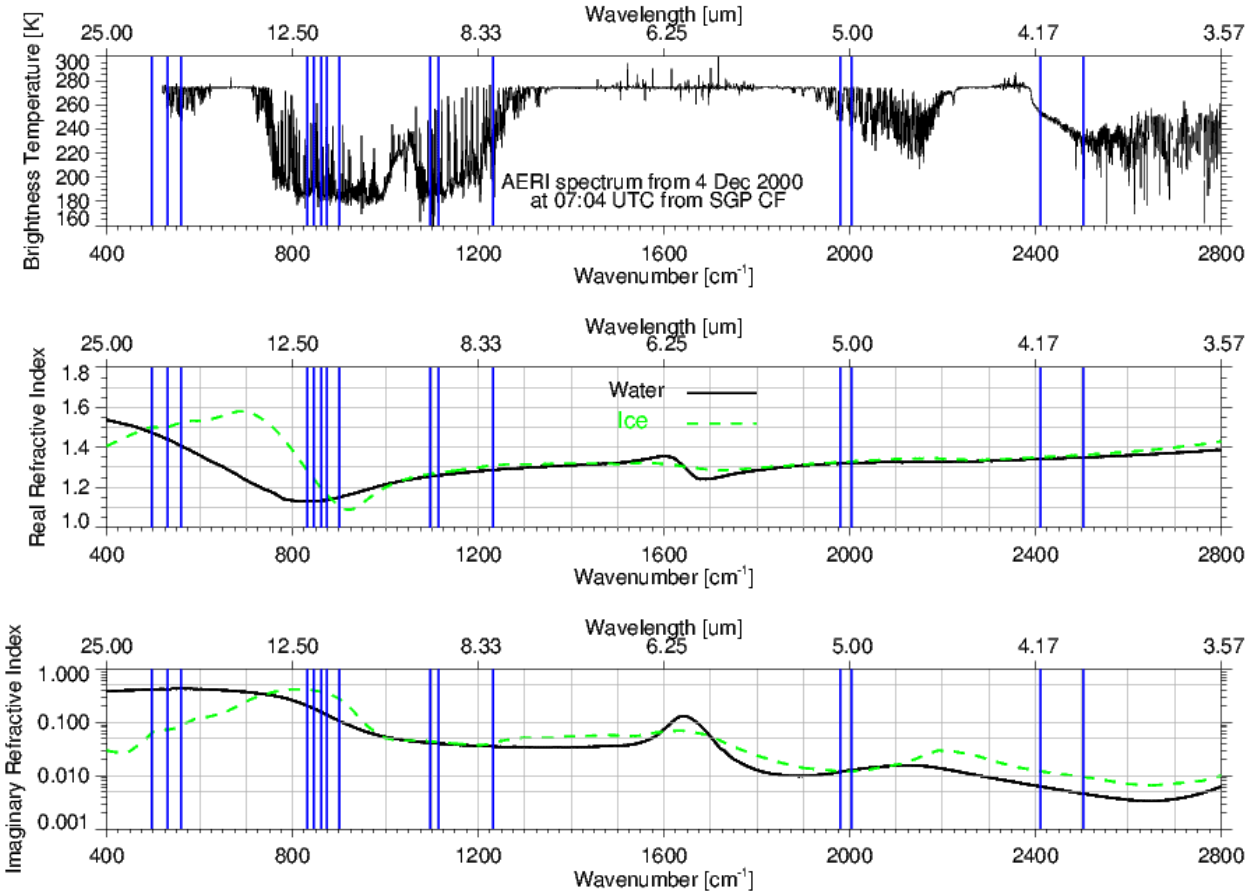

Figure 1. Typical clear-sky brightness temperature spectrum observed from the AERI at SGP for 1 cm of percipitable water vapor (PWV). The refractive indices of ice and liquid water are also shown as a function of wavelength. Note that the extended range AERIs deployed at NSA and SHEBA make observations out to 24 μm.

observations made by the cloud particle imager (CPI) flown on the National Center for Atmospheric Research (NCAR) C-130 during the First ISCCP (International Satellite Cloud Climatology Program) Regional Experiment-Aerosol Characterization Experiment (FIRE-ACE). Both phases used a gamma size distribution, again suggested by the CPI observations. The ice particles were modeled as hexagonal columns (Yang et al. 2001) for this simulation, but modeling the ice as spherical particles (using Mie code) does not significantly affect the results. The lower portion of the figure indicates the makeup of the clouds in the simulation. The first sample was a clear-sky case. The next 11 samples are for all ice clouds (blue symbols) with optical depths ranging from 0.1 to 8.0. The next 11 samples are for liquid water clouds (red symbols) with optical depths again ranging from 0.1 to 8.0. The remaining samples are all mixed phase. For each of the 11 intervals, the total optical depth of the cloud is fixed, with the fraction of the total optical depth attributed to ice ranging from 0.1 to 0.9. The upper panel of the figure shows various brightness temperature differences between the three channels used in the retrieval. The results of the phase determination algorithm are shown along the top of the top panel. Blue symbols indicate ice-only cloud, red symbols indicate a liquid-only cloud, green symbols indicate a mixed phase cloud, and purple symbols indicate that the cloud is too opaque for the algorithm to decide. The

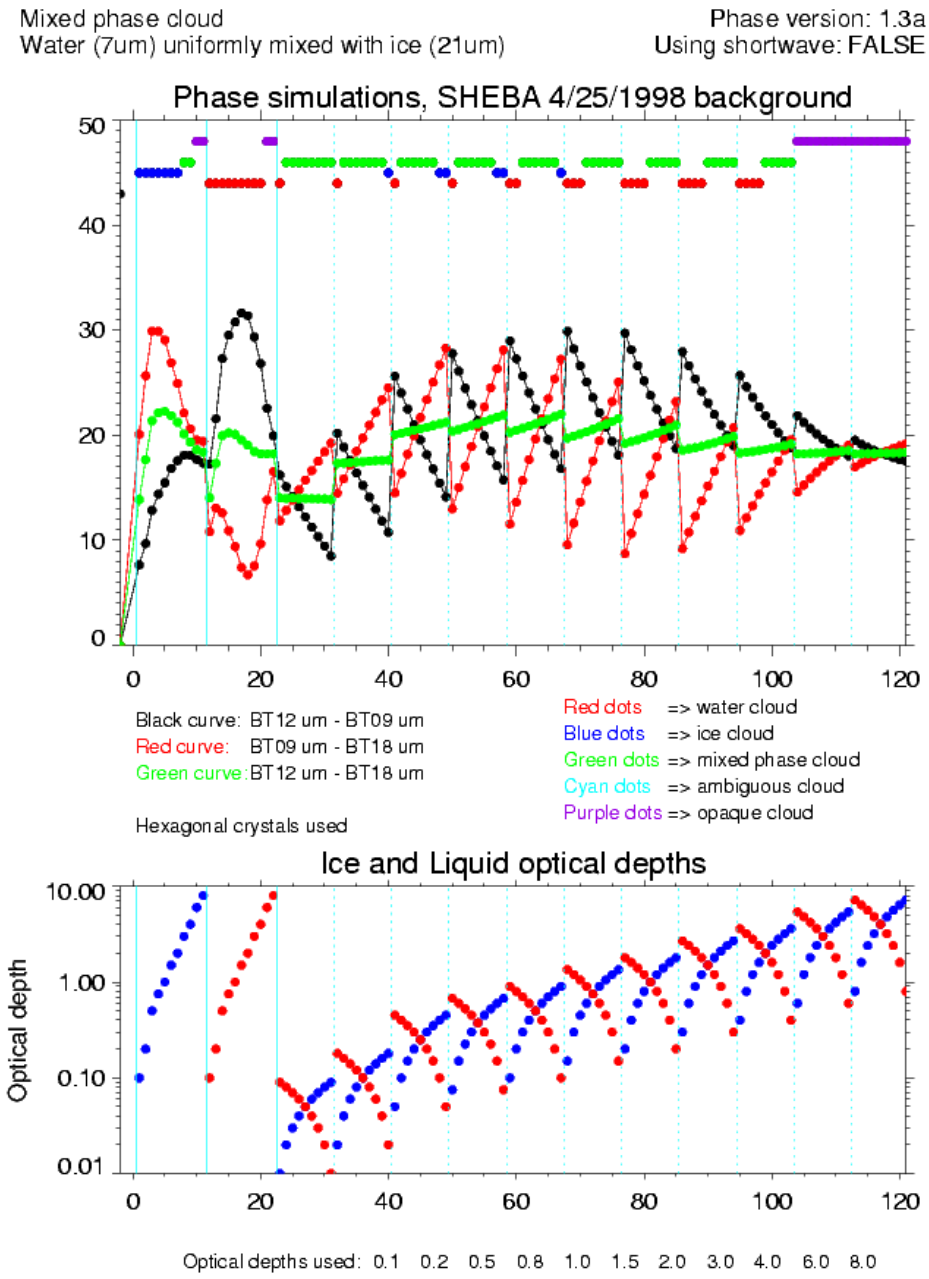

Figure 2. Results from the mixed-phase cloud simulation to test the prototype cloud phase detection algorithm designed to use AERI radiance observations. See text for details.

three-channel algorithm performs admirably for a majority of the mixed-phase cases, with errors in phase determination occurring when the cloud is mostly one phase. For example, when the liquid water optical depth is 90% of the total optical depth, the algorithm tends to call the cloud all liquid water versus mixed phase. The sensitivity of the phase determination algorithm to particle size of liquid and ice particles has been investigated with similar results for most reasonable effective radii. The technique is limited to optical depths less than approximately five, but it is at these small optical depths that the

combined radar/Microwave Radiometer (MWR) techniques tend to lose their sensitivity, primarily due to the sensitivity of the MWR. Therefore, this technique would be a valuable addition to the traditional radar/MWR techniques.

Initial Results

The first step required before utilizing the IR for cloud property studies, especially when the clouds are optically thin like many clouds in the Arctic, is to evaluate the ability to model the clear-sky. Comparisons between AERI observed and LBLRTM calculated radiance show a significant 1 mW/(m^2 ster cm^{-1}) residual in the 8-13 μm window. This cannot be explained by uncertainties in the water vapor amount or the continuum absorption (Figure 3a). This radiance residual translates into a 20-30 K error in brightness temperature. However, by inserting an ice cloud at the surface, with an effective radius of 50 μm and a small optical depth, explains the residuals fairly well. Using an iterative technique, the required cloud optical depth and effective radius was retrieved for each of the "confirmed" clear-sky samples (using Millimeter Wave Cloud Radar [MMCR] and Depolarization Aerosol and Backscatter Unattended Lidar [DABUL] data) during SHEBA (Figure 3b). In all cases, the

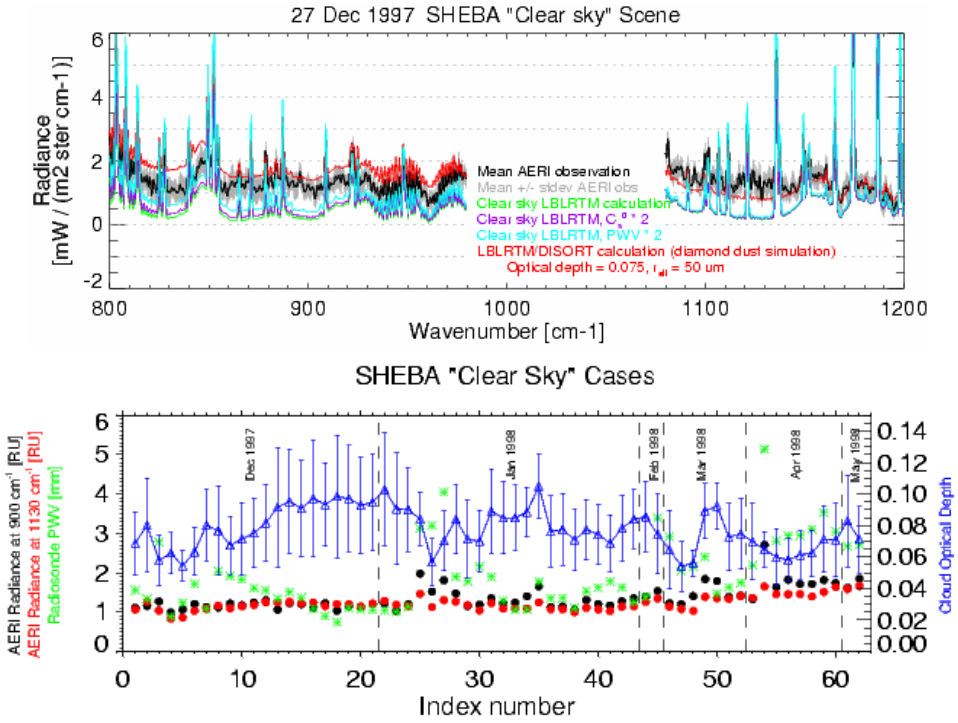

Figure 3. a) "Clear-sky" comparison of observed minus calculated downwelling radiance. Large perturbations of the PWV used in the calculation, or the water vapor continuum absorption, does not explain the discrepancy between the observation and calculation. An optically thin ice cloud at the surface can explain these residuals. b) Retrieval of ice cloud optical depth needed to match the AERI observations for 62 confirmed "clear-sky" scenes (using MMCR/DABUL data) during SHEBA.

effective radius was 50 μm or greater, and the optical depth varied at values less than 0.1. These values agree with diamond dust values reported by Whitte (1968). We are investigating the observations to rule out calibration uncertainties.

The AERI phase determination algorithm was applied to several days of data collected during SHEBA. An example of the results is shown in Figure 4 for April 21, 1998. On this day, a small surface low was situated northeast of the ship. Winds were light and easterly at the surface, with stronger winds from the southwest at upper levels. The DABUL lidar data, shown in Figure 4, indicate a single-layer cloud existed from 9-17 Universal Time Coordinates (UTC) with depolarization values ranging from 20% to 30%. These values are typically associated with scattering due to ice. The AERI phase detection algorithm indicated this cloud was a mixed phase cloud, which is certainly possible due to the temperature of the cloud (~ -20K). From 17 to 24 UTC, a lower level cloud with low depolarization (which is usually associated with scattering from spherical liquid water drops) was overhead, along with the upper level cloud with higher depolarization ratios that was becoming more porous. For times when the upper level cloud wasn't directly overhead, the AERI phase detection algorithm indicated the scene (which consisted only of the lower level cloud) was liquid water, while periods when both cloud levels where in the scene were identified as mixed phase.

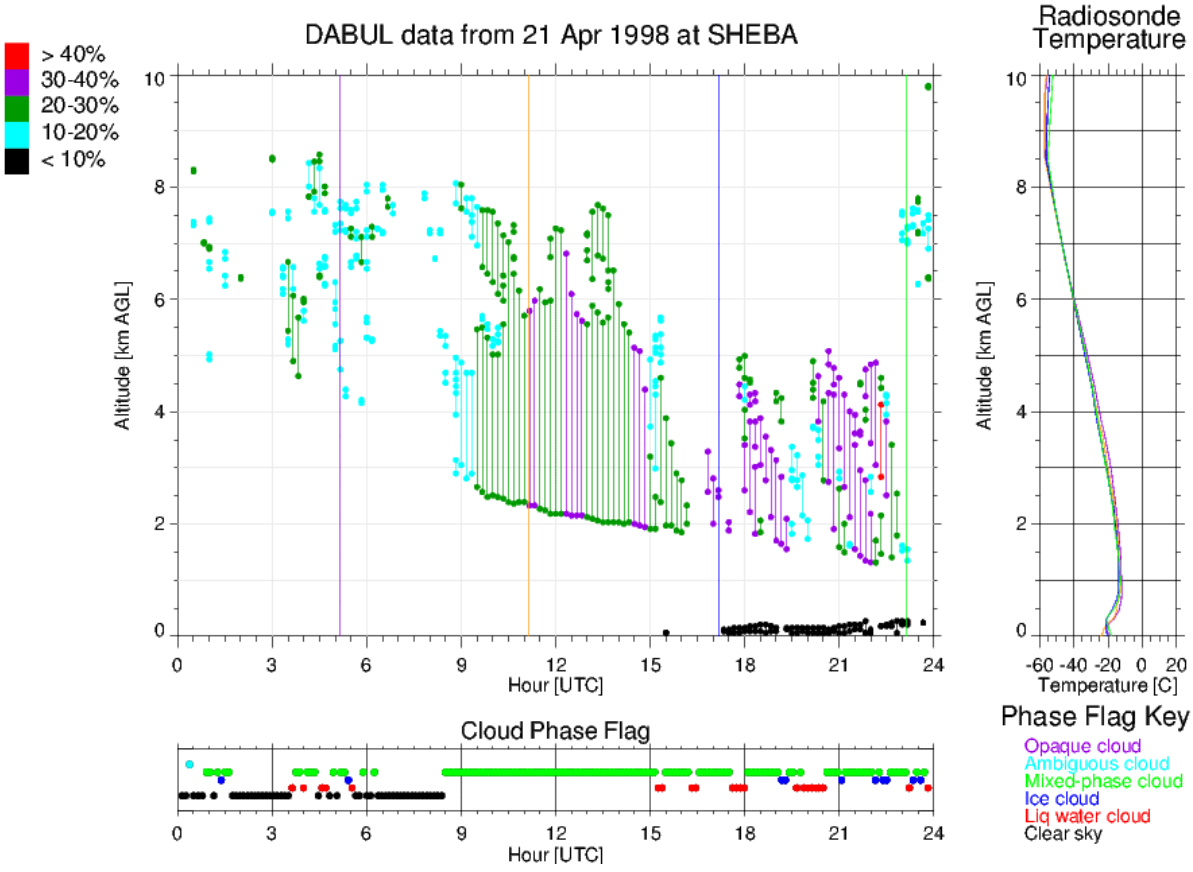

Figure 4. Results of the AERI phase determination algorithm, together with DABUL depolarization data and radiosonde temperature profiles, for April 21, 1998.

Future Work

As indicated above, this technique currently uses only data at three wavelengths, and therefore does not take advantage of the high spectral resolution of the AERI (other than avoiding spectral regions that have significant absorption features of water vapor and other molecules). We are moving to extend this technique to include multiple wavelengths, including wavelengths in the 3-5 μm region where the refractive index of water and ice differ as compared to the 8-13 μm region to increase the sensitivity of the algorithm. We will also incorporate the cloud boundary information from the lidar and cloud radar to facilitate the retrieval of cloud liquid and ice water paths and effective radii. These data will then be used to build monthly and seasonal climatologies for the Arctic, using data from the SHEBA and ARM NSA sites.

Acknowledgments

This work was funded by the ARM Program. We thank Ping Yang for the scattering properties of the hexagonal columns and Bryan Baum for helpful discussions. The DABUL data were acquired from the SHEBA data archive on the UCAR Joint Office for Science Support (JOSS) webpage.

Corresponding Author

Dave Turner, dturner@ssec.wisc.edu.

References

Baum, B. A., P. F. Soulen, K. I. Strabala, M. D. King, S. A. Ackerman, W. P. Menzel, and P. Yang, 2000: Remote sensing of cloud properties using MODIS airborne simulator imagery during SUCCESS: 2. Cloud thermodynamic phase. *J. Geophys. Res*., **105**, 11781-11792.

Curry, J. A., W. B. Rossow, D. Randall, and J. L. Schramm, 1996: Overview of Arctic cloud and radiation characteristics. *J. Climate*, **9**, 1731-1764.

Whitte, H. J., 1968: Airborne observations of cloud particles and infrared flux density in the Arctic. MS Thesis, Dept. of Atmos. Sci., p. 102, University of Washington.

Yang, P., B. Gao, B. A. Baum, Y. X. Hu, W. J. Wiscombe, S. Tsay, D. M. Winker, and S. L. Nasiri, 2001: Radiative properties of cirrus clouds in the infrared (8-13 μm) spectral region. *J. Quant. Spec. Rad. Trans*., **70**, 473-504.